Surface Science of Elastomeric Coatings Prepared from α,ω-Dihydroxypoly(dimethylsiloxane) and the Ethoxysiloxane Mixture "ES40"

Janelle Uilk,[†,‡] Steve Bullock,[‡] Erika Johnston,[‡,⊥] Sharon A. Myers,[§,#] Larry Merwin,[§] and Kenneth J. Wynne*[,†]

Chemical Engineering Department, School of Engineering, Virginia Commonwealth University, 601 West Main St., Richmond, Virginia 23284-3028; Naval Research Laboratory, Materials Chemistry Branch, Code 6120, Washington, D.C. 20375; and Naval Air Warfare Center, Weapons Division, Chemistry and Materials Branch, China Lake, California 93555

Received January 7, 2000; Revised Manuscript Received July 25, 2000

ABSTRACT: Hybrid poly(dimethylsiloxane) networks have been prepared with the ethoxysiloxane mixture "ES40" that acts as a cross-linker and siliceous domain (SD) precursor through sol−gel chemistry. ES40, with an approximate formula $(SiO(OEt)_2)_n$, is a mixture of oligo-ethoxysiloxanes that is much less volatile than tetraethoxysilane (TEOS) and provides hybrid elastomeric coatings of reproducible composition. With SiOEt from ES40 and SiOH from $HO(Me_2SiO)_nH$, compositions with SiOEt/SiOH ratios from 5 to 35 (ES40-5x−ES40-35x) were prepared. Solid-state ^{29}Si NMR spectroscopy was used to determine the relative amounts of PDMS and SD in the hybrid elastomers. The relative amounts of Q^2, $(\equiv SiO)_2\mathbf{Si}(OH)_2$; Q^3, $(\equiv SiO)_3\mathbf{Si}(OH)$; and Q^4, $(\equiv SiO)_4\mathbf{Si}$, in the SD were estimated by deconvolution of the ^{29}Si NMR peaks. Both light microscopy and tapping mode atomic force microscopy (TM-AFM) show that PDMS-SD compositions "5x" and higher slowly develop "island-like" surface features while stored at ambient conditions. After 1 month cure, PDMS-SD surface features are ≤1 μm, while after 6 months feature size is broadly distributed up to ∼10 μm. In contrast, surface features developed quickly (24 h) with previously reported PDMS-FSD hybrids, where FSD is fluorinated siliceous domain, from (tridecafluoro-1,1,2,2-tetrahydrooctyl)triethoxysilane. AFM experience demonstrates that PDMS-SD surface features are often poorly adherent and easily moved compared to the robust phase-separated surface structure of PDMS-FSD materials. Differing dynamic contact angle (DCA) analysis protocols with water as the interrogating fluid show that water contamination affects force vs distance curve (fdc) data for PDMS-SD hybrids. Intrinsic wetting behavior for PDMS-SD hybrids is reproduced only with a protocol where clean water is used for each DCA cycle. The stability in water of PDMS-SD materials is strongly compositionally dependent. Over a period of 70 days, the ES40-14x composition showed the greatest resistance to mass loss with a mass loss rate of 0.08 wt %/month.

Introduction

This research is part of a program directed at understanding and controlling the surface chemistry, stability, and morphology of PDMS-containing elastomers. Gaining understanding of surface morphology and chemical stability of hybrid PDMS elastomers is important to the development of improved biocompatible materials and nontoxic fouling release coatings.[1−3] In this context, we have explored strategies for minimizing adhesion of prospective settling organisms to a coated substrate. To reduce van der Waals and hydrogen-bonding interactions between the coating and prospective adherent organisms, we have focused on reduction of coating surface free energy.[4]

Silicone coatings are typically generated in air wherein the surface free energy is minimized by the presence of a surface PDMS domain. On immersion, however, retention of the noninteracting, low surface free energy PDMS surface domain is compromised by the polar nature of water and thermodynamically driven processes that bring polar functionality to the polymer−water interface.[1] The extent of physical change that occurs at the water−silicone interface is determined by accessibility of polar functionality to water and the nature of available functionality (chain ends, domain fragments, etc.).[5] It is likely that polar surface functionality improves adhesion of fouling organisms. Thus, we seek methods that favor stabilizing elastomeric surfaces against processes that create polar surface functionality.

Another consideration is the mechanics of adhesion; Chaudhury[6] and Kohl[7] have used principles delineated many years ago by Kendall[8] to show that adhesion is minimized by reducing coating modulus and maximizing coating thickness. The combination of low modulus and low surface free energy accounts in large part for silicones being favored as noninteracting biomedical elastomeric materials.[9]

For applications requiring constant immersion in aqueous media, the chemical stability of silicones is important but often not considered. It is usually assumed that chemical stability is excellent, but subtle aspects are important and not well understood. For

[†] Virginia Commonwealth University.
[‡] Naval Research Laboratory.
[§] Naval Air Warfare Center.
[⊥] Current address: Genzyme Corporation, One Kendall Square, Cambridge, MA 02139.
[#] Current address: Bauch and Lomb Corporation, 1400 N. Goodman St., Rochester, NY 14604.

10.1021/ma000023y CCC: $19.00
Published on Web 11/14/2000

example, one chemical stability issue is the diffusion of species from the network into the surrounding medium. The diffusion of silicone species from the network to the surface of the polymer and thence into the environment may be helpful to some applications such as fouling release coatings.[10] However, the diffusion of silicone species into the environment of implants is undesirable.[11]

In exploring the polymer surface science of PDMS elastomers, we have examined ethoxysilane cured hydroxy-terminated PDMS, $HO(Me_2SiO)_nH$.[12,13] Previous work on alkoxysilane cured PDMS systems has emphasized the self-reinforcing nature of the "precipitated" siliceous domain.[14] Other work has examined the bulk morphology of PDMS-SD materials.[15,16] Interest in the surface morphology of alkoxysilane cured PDMS has been more recent. The cure of $HO(Me_2SiO)_nH$ with fluorinated alkoxysilanes yields poly(dimethylsiloxane)-fluorinated siliceous phase (PDMS-FSP) materials that display compositionally dependent surface morphologies.[13,17] Tetraethoxysilane (TEOS) and tetramethoxysilane (TMOS) cured low molecular weight $HO(Me_2SiO)_nH$ with rather high catalyst concentrations (5−10%) gave surface structures that appear bicontinuous.[18,19]

The present paper describes PDMS-SD coatings in which the ethoxysiloxane mixture "ES40", with the approximate formula $(SiO(OEt)_2)_n$, is used as the SD precursor and cross-linker for $HO(Me_2SiO)_nH$. ES40 is an oligo-ethoxysiloxane mixture[20] that is much less volatile than TEOS. Our synthetic method avoids the use of solvents such as ethanol/water and relies on the relative involatility of ES40 for obtaining hybrid elastomeric coatings with reproducible compositions. We report that these optically transparent coatings show slow emergence of unexpected surface features characterized by tapping mode atomic force microscopy (TM-AFM). The nature of these features is compared to those observed in hybrid PDMS coatings generated with $CF_3(CF_2)_5(CH_2)_2Si(OEt)_3$.[13] Wetting behavior is examined as a measure of physical and chemical surface stability over short immersion times involved in dynamic contact angle experiments. Finally, the compositionally dependent long-term stability in water of these coatings is presented.

Experimental Section

Materials Preparation. α,ω-Hydroxy-terminated poly(dimethylsiloxane), $HO(Me_2SiO)_nH$ (Gelest Corp., Tullytown, PA), was used as received for most compositions: M_w, 18 kDa by GPC vs polystyrene, $M_w/M_n = 2.0$. One series of samples was made with acetone extracted $HO(Me_2SiO)_nH$. Extraction was done in an attempt to remove cyclics and short-chain linear species from the $HO(Me_2SiO)_nH$. Acetone (0.3 L) was added to 0.1 L of $HO(Me_2SiO)_nH$ in a 0.5 L separatory funnel. The mixture was agitated, and the PDMS-rich lower layer was removed. Acetone was allowed to evaporate in a hood, and then the procedure was repeated three times: M_w, 24 kDa; $M_w/M_n = 1.7$.

Dibutyltin diacetate (DBTDA, Aldrich) was employed as the hydrolysis−condensation catalyst. For unextracted $HO(Me_2SiO)_nH$, 0.18 wt % DBTDA was used. For extracted $HO(Me_2SiO)_nH$, either 0.5 or 0.18 wt % DBTDA was utilized. Compositions prepared with 0.5 wt % DBTDA required an initial mixing time 2−3 times shorter than those prepared with 0.18 wt % catalyst.

With SiOEt from ES40 and SiOH from $HO(Me_2SiO)_nH$, compositions with SiOEt/SiOH ratios from 5 to 35 (ES40-5x−ES40-35x) were prepared. A representative procedure for preparation of coated slides for PDMS-SD composition "10x" follows. As-received $HO(Me_2SiO)_nH$ (13.3 g) was poured into a tared 50 mL beaker. ES40 was added dropwise (0.66 g, 5 wt %) followed by DBTDA catalyst (0.022 g, 0.18 wt %). The viscous solution was stirred mechanically until the resin thickened (2.7 h). The mixture was then degassed in a vacuum oven at ambient temperature for 10 min. Part of the resin (2.2 g) was poured into a Petri dish (55 × 11 mm); this material was used for solid-state NMR experiments. The remainder was used for coating slides. The resin was dip-coated onto flame-dried glass microscope coverslips (22 × 40 × 0.15 mm) with a single coat. Care was taken to ensure an even coating on the slides. The coatings were cured at room temperature (for at least 1 month) with the slides in a vertical orientation (coated portion uppermost). Samples were cured in 90% relative humidity, which was achieved using an inverted beaker enclosing a container of water. Samples were subsequently stored at ambient temperature and humidity.

To obtain a siliceous phase with the highest possible Si content for ^{29}Si NMR spectroscopy, a sample of ES40 was allowed to "self-cure". DBTDA (0.25 wt %) was added to a sample of ES40. The sample gelled after few hours, and a brittle glass formed after overnight cure.

Solid-State Nuclear Magnetic Resonance (NMR) Spectroscopy. Solid-state ^{29}Si NMR magic angle spinning (MAS) spectra were acquired with a Bruker MSL-200 operating at 39.8 MHz for silicon. Single-pulse excitation spectra were recorded with 600 acquisitions for the self-cured ES40 samples while PDMS-SD samples were recorded with 2600−2800 acquisitions. Recycle delays of 120 s and MAS speeds of 2.0−2.1 kHz were used. All spectra were acquired at ambient temperature and externally referenced to octakis(trimethylsiloxy)silsesquioxane (Q8M8) at 11.9 ppm.

Light Microscopy. Optical micrographs were taken with a Zeiss Axiotech light microscope fitted with a 50× objective and a MC80 Polaroid camera attachment. Exposure times were determined by the Zeiss control module.

Atomic Force Microscopy (AFM). Samples were imaged with a Digital Instruments (Santa Barbara, CA) Nanoscope IIIa with a Multimode head. Topographic and phase contrast imaging on all samples were performed by means of TM-AFM (tapping mode atomic force microscopy). Nanoprobe cantilevers (225 μm, Digital Instruments) were utilized. Samples were cut from coated slides, rinsed with HPLC grade methanol followed by deionized water, and dried with filtered nitrogen gas. Phase contrast AFM was carried out at a set-point amplitude to cantilever free-oscillation amplitude (A_{sp}/A_0) ratio of 0.8, generally regarded as low tapping force.[21] The drive amplitude was generally 250 mV, and imaging was conducted just below the cantilever resonant frequency of 170−180 kHz. Phase imaging was done at 0° phase offset, which optimized phase contrast.

Dynamic Contact Angle (DCA) Analysis. Contact angle analysis was performed with a Cahn model 312 dynamic contact angle (DCA) analyzer (Cerritos, CA), which uses the Wilhelmy plate method.[22] The instrument's surface tension quantification limit is 0.1 dyn/cm. The probe liquid was deionized water (18 MΩ·cm) from a Barnstead (Dubuque, IA) Nanopure system. The surface tension of the probe liquid was checked daily and was typically 72.6 ± 0.1 dyn/cm.

In DCA experiments, a coated slide is immersed and withdrawn from the interrogating liquid (water). Thus, a large fraction of the sample surface is examined. In DCA analysis, the linear portion of each force−distance curve (fdc) allows calculation of advancing contact angle, θ_{adv}, and receding contact angle, θ_{rec}.

Two protocols were used in DCA analysis (see Discussion). The first protocol produces four fdc's from a ∼1.2 cm travel distance and 10 s dwell times before sample immersion and withdrawal. Travel speed for these measurements was 100 μm/s. The second protocol recorded six fdc's from a travel speed of 100 μm/s and dwell times of 10 or 20 s between sample immersion and withdrawal. Ten second dwell times between immersion and withdrawal were used for cycles 3, 4, and

5. During the 20 s dwell times between immersion and withdrawal for cycles 1, 2, and 6 the beaker and water used for the previous fdc was removed and replaced by a clean beaker and water.

Mass Loss in Water. Mass loss was determined on a weekly basis with three replicates used per sample set. Samples were removed weekly from 100 mL of water containing 200 ppm sodium azide as a biocide,[23] rinsed with 18 MΩ·cm Nanopure water, dried for 30 s with forced air, further dried in air for 1 h, and weighed. Initial film masses (0.5−0.8 g) were calculated by subtracting the mass of the glass coverslips, which were flame-dried and weighed prior to coating, from the mass of each sample. Samples that were allowed to dry overnight weighed nearly the same as those allowed to dry for 1 h. After weekly removal of the sample from azide−water and examination of mass, the samples were reimmersed in fresh Nanopure azide−water.

Results and Discussion

Network Formation. ES40 is comprised of a mixture of linear and cyclic ethoxysiloxanes with the approximate empirical formula $(SiO(OEt)_2)_n$.[24,25] ES40 has three advantages compared to TEOS as a siliceous phase precursor/cross-linker in the preparation of coatings. (1) The relative involatility of ES40 compared to that of TEOS results in PDMS-SD materials whose compositions agree with calculated values from reactant masses. This is important for an accurate knowledge of the relative amounts of PDMS and siliceous domains. With our synthetic approach, cure is slow due to the absence of solvent (e.g., ethanol/water) and reliance on ambient water vapor to effect hydrolysis. Tack-free films are obtained in a few hours, but about 24 h is required for complete ethanol evolution (eq 1a).[13] In contrast, under these cure conditions, up to 90% loss of TEOS occurs depending on the processing procedure.[12] (2) Less shrinkage occurs with ES40 because only 2 mol of ethanol is released per Si (eq 1a), whereas 4 mol of ethanol is released per Si in TEOS. (3) The lower ethanol release for ES40 means less "volatile organic compound" (VOC) evolution and safer processing conditions, as ethanol is flammable.

Networks were prepared though the DBTDA-catalyzed reaction of ES40 and 26 kDa hydroxy-terminated PDMS. The mechanism of catalysis is unknown, but dibutyl tin dialkanoates are routinely used for alkoxysilane cure.[26] A minimum catalyst concentration (ca. 0.2 wt %) was used for most compositions. The odor of acetic acid is noted in film preparation. The evolution of acetic acid suggests that the $[Bu_2SnO]$ moiety is incorporated in the network, probably through the formation of Si−O−Sn bonds. Thus, minimizing catalyst concentration minimizes possible effects on morphology, surface properties, and stability.

Cure is not observed in a dry atmosphere; exogenous water is required. A simplified view of cure chemistry is represented by eqs 1a−1d. The formula of ES40 is represented by $SiO(OEt)_2$. Equation 1a shows the hydrolysis of ES40 while eq 1b depicts self-condensation to SiO_2. Equation 1c shows the reaction of ES40 with $HO(Me_2SiO)_nH$ while eq 1d shows the reaction of hydrolyzed ES40 with $HO(Me_2SiO)_nH$. Equations 1a−1d show approximate product stoichiometry because under conditions of ambient temperature cure the SD is not SiO_2. ^{29}Si NMR experiments discussed below show that varying Si−OH mole fractions are present depending on composition. Equations 1a and 1b show that 1 g-atom of O is incorporated into the SD for every mole of water utilized in hydrolysis.

Table 1. Proportions of Polymer (PDMS) and Ethoxysilane (ES40) Used To Prepare PDMS-SD Networks

sample designation	mass ES40(g) (wt %)	mass PDMS(g) (wt %)	ethoxy/hydroxy (mol/mol)
ES40-5x	0.346 (2.4)	14.352 (97.4)	4.7
ES40-10x	0.661 (5.0)	13.294 (94.8)	9.6
ES40-12x	0.814 (6.0)	13.573 (93.8)	11.6
ES40-14x	1.010 (7.2)	13.960 (92.6)	14.0
ES40-19x	1.118 (9.6)	11.671 (90.2)	18.6
ES40-28x	2.233 (14.5)	15.429 (85.3)	28.0
ES40-35x	2.542 (18.1)	14.083 (81.7)	35.0

Network formation by ES40 (DBTDA catalyst):

$$SiO(OEt)_2 + 2H_2O \rightarrow SiO(OH)_2 + 2EtOH \quad (1a)$$

$$SiO(OH)_2 \rightarrow SiO_2 + H_2O \quad (1b)$$

$$SiO(OEt)_2 + HO(Me_2SiO)_nMe_2SiOH \rightarrow [SiO][-O(Me_2SiO)_n-] + 2EtOH \quad (1c)$$

$$SiO(OH)_2 + HO(Me_2SiO)_nMe_2SiOH \rightarrow [SiO][-O(Me_2SiO)_n-] + 2H_2O \quad (1d)$$

In a composition such as "ES40-5x", the "5" denotes the initial SiOEt/SiOH ratio where all SiOEt derives from ES40. ^{29}Si NMR spectroscopy shows that about 8% TEOS is present in ES40, so mass loss via TEOS volatilization is decreased substantially compared to use of TEOS alone.[12,24] Table 1 lists the amounts of reactants for compositions prepared in this study. Below, we use integrated ^{29}Si NMR data to assess the Si_{PDMS}:Si_{SD} ratio and compare these data with those calculated from mass of reagents.

^{29}Si NMR Spectroscopy. Solid-state ^{29}Si NMR spectroscopy was used to characterize the composition of representative samples and to speciate the SD. Figure 1A−D shows the ^{29}Si NMR spectra obtained for (A) ES40-5x, (B) ES40-14x, (C) ES40-28x, and (D) $SiO_{2-n/2}(OH)_n$ resulting from the hydrolysis and condensation polymerization of ES40 alone.

The spectra for the PDMS-SD materials (Figure 1A−C) show a large peak for $(Me_2\mathbf{Si}O)_n$ at −22.4 ppm. The peak at −76.4 ppm is a spinning sideband associated with $(Me_2\mathbf{Si}O)_n$. The remainder of the peaks are assigned to silicons in the SD according to the Q^n designation[27] where the formula $\mathbf{Si}(OH)_{4-n}(OSi\equiv)_n$ is used to generate the three Si local environments (Q^2, Q^3, Q^4). Q^2, Q^3, and Q^4 chemical shifts for ES40-5x, -14x, and -28x compositions are listed in Table 3. Assignment of peak positions is consistent with previous literature: −95 to −75 ppm for Q^2, −104 to −91 ppm for Q^3, and −120 to −108 ppm for Q^4.[28−31]

The relative amounts of $(Me_2SiO)_n$ and SD were estimated by spectral integration. The results are compared with compositions determined from measured masses of starting materials in Table 2. The Si_{PDMS}:Si_{SD} ratio from NMR integration is systematically lower compared with the compositions estimated from mass

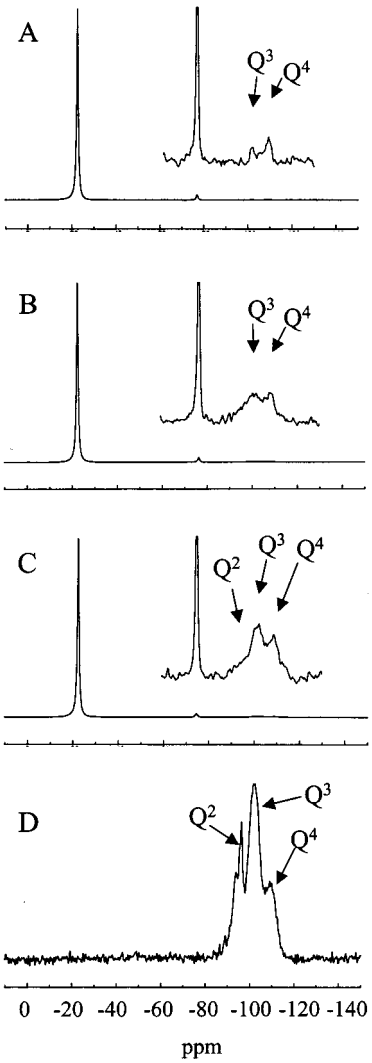

Figure 1. Solid-state ^{29}Si NMR spectra of (A) ES40-5x, (B) ES40-14x, (C) ES40-28x, and (D) self-cured ES40. Insets are expanded and amplified regions for siliceous phase silicon resonances.

Table 2. Ratios of PDMS and SD Silicon Atoms Calculated from ^{29}Si NMR Integration and Measured Mass

ES40 sample designation	from NMR integration data	from measured mass
5x	86	74
14x	27	25
28x	19	13

measurements. The greatest deviation is seen for ES40-28x, where NMR gives a Si_{PDMS}:Si_{SD} of 19 while a ratio of 13 is calculated from initial mass of reagents. ES40 contains 8 wt % TEOS, so volatilization of TEOS probably accounts for most of the difference between the NMR and mass data.[12,24] The relatively broad ^{29}Si peaks, noise level, and long signal acquisition times may also account for some of the discrepancy.

The insets in Figure 1A−C show amplified ^{29}Si SD peaks. Figure 1A shows a spectrum of ES40-5x where SD peaks at −102.6 and −108.5 ppm are due to Q^3 and Q^4, respectively. The SD ^{29}Si NMR peaks were deconvoluted to estimate the relative amounts of Q species (Table 3). The line shapes were fit with a mixed Gaussian/Lorentz function. As seen in Table 3, the SD in ES40-5x is comprised of 69% Q^3 and 31% Q^4. The spectrum of the ES40-14x sample shown in Figure 1B has peaks at −102.6 (Q^3, 85%) and −108.5 ppm (Q^4, 15%). Figure 1C shows the spectrum of ES40-28x that has a shoulder centered at −93.8 ppm (Q^2, 17%) and relatively broad peaks centered at −101.3 ppm (Q^3, 41%) and −108.7 ppm (Q^4, 42%).

Figure 1D shows the ^{29}Si NMR spectrum of the glass from hydrolysis and condensation of ES40 alone. Three peaks are observed at −96.5 (Q^2, 30%), −101.9 ppm (Q^3, 53%), and −109.1 ppm (Q^4, 17%). If the empirical formulas $SiO(OH)_2$, (Q^2), $SiO_{1.5}(OH)$ (Q^3), and SiO_2 (Q^4) are used, the self-cured ES40 glass may be represented by $(SiO(OH)_2)_{0.26}(SiO_{1.5}OH)_{0.53}(SiO_2)_{0.20}$. This can be further reduced to $Si(-OSi\equiv)_{2.9}(OH)_{1.1}$ or $SiO_{1.45}(OH)_{1.1}$. Thus, about one in four sites on Si in the SD is occupied by OH groups.

In a similar way, empirical formulas for the SD may be calculated for the PDMS-SD materials (Table 4). ES40-14x and -28x have Si(−OSi≡)/(OH) ratios (3.8−5.0) similar to that for the ES40-derived glass. However, the Si(−OSi≡)/(OH) ratio for ES40-5x is substantially higher. Apparently, compositions with OEt/OH ratios approaching stoichiometry change the distribution of Q species in the siliceous domain. Alternatively, the low fraction of SD in ES40-5x may have affected the detection of Q^2.

Optical Microscopy. Initially, the PDMS-SD elastomeric coatings and bulk samples are optically transparent.[32] The refractive index of PDMS is 1.403.[33] The refractive index of the SD is unknown, but the n_d for ES40 liquid (1.397) and that for quartz (1.544)[34] provide lower and upper limits. It is likely the SD has a refractive index closer to quartz than to ES40 liquid. Given the unlikely chance that the SD and PDMS domains have the same refractive index, the optical transparency of the *bulk* is due to domain sizes for PDMS and SD that are smaller than optical wavelengths. This is in accord with results reported by Wilkes on TEOS cured PDMS.[15]

After cure, when coatings age in air, a slight haze develops. Figure 2 shows optical micrographs of ES40-5x, -12x, and -35x samples that have been aged for 7 months. Surface features ranging in size up to 5 μm appear as faint, diaphanous circular objects. Comparing parts A and B of Figure 2, it is seen that the area fraction of these features increases somewhat with increasing SD content. These features have been further characterized by TM-AFM as described in the next section.

Atomic Force Microscopy. The study of the surface morphology of polymers using atomic force microscopy (AFM) is a rapidly growing area.[35] In addition to height imaging, phase imaging allows differentiating surface features by modulus differences.[36−38]

The unexpected development of surface features on PDMS-SD materials is shown in parts A and B of Figure 3, which provides images of ES40-10x at 1 and 6 months, respectively. At 1 month, surface features are no larger than ~1 μm, whereas after 6 months sizes are broadly distributed to about ~10 μm. These results may be compared to those of Viers et al.,[19] who prepared PDMS-SD materials with stoichiometric amounts of various alkoxysilanes as the SD precursor, low MW α,ω-dihydroxy-functionalized PDMS resin, and 5−10% tin(II) octoate or dibutyltin dilaurate as catalysts. The materials prepared by Viers et al. exhibited a relatively rapid onset of "post-gel turbidity", indicating bulk phase separation. The morphological observations are different

Table 3. ^{29}Si NMR Spectroscopy Data

sample designation	Q^2 peak				Q^3 peak				Q^4 peak			
	δ (ppm)	int	area	%	δ (ppm)	intensity	area	%	δ (ppm)	int	area	%
ES40-5x					−102.6	0.40	30	31	−108.5	0.67	67	69
ES40-14x					−100.9	1.1	330	85	−108.4	0.65	59	15
ES40-28x	−93.8	0.80	136	17	−101.3	3.1	340	41	−108.7	2.4	350	42
self-cured	−96.5	17	1400	30	−101.9	18	2500	53	−109.1	6.8	820	17

Table 4. Composition of the Siliceous Domain Determined by Integration of the ^{29}Si NMR Spectroscopy Data in Figure 1

sample designation	mole fraction			$Si(-OSi\equiv)_m(OH)_n$	$Si(-OSi\equiv)/(OH)$	$SiO_m(OH)_n$
	Q^2	Q^3	Q^4			
ES40-5x	0	0.28	0.72	$Si(-OSi\equiv)_{3.72}(OH)_{0.28}$	13	$SiO_{1.86}(OH)_{0.28}$
ES40-14x	0	0.83	0.17	$Si(-OSi\equiv)_{3.17}(OH)_{0.83}$	3.8	$SiO_{1.59}(OH)_{0.83}$
ES40-28x	0.14	0.39	0.47	$Si(-OSi\equiv)_{3.33}(OH)_{0.67}$	5.0	$SiO_{1.14}(OH)_{0.67}$
ES40 self-cured	0.26	0.53	0.20	$Si(-OSi\equiv)_{2.91}(OH)_{1.09}$	2.6	$SiO_{1.45}(OH)_{1.1}$

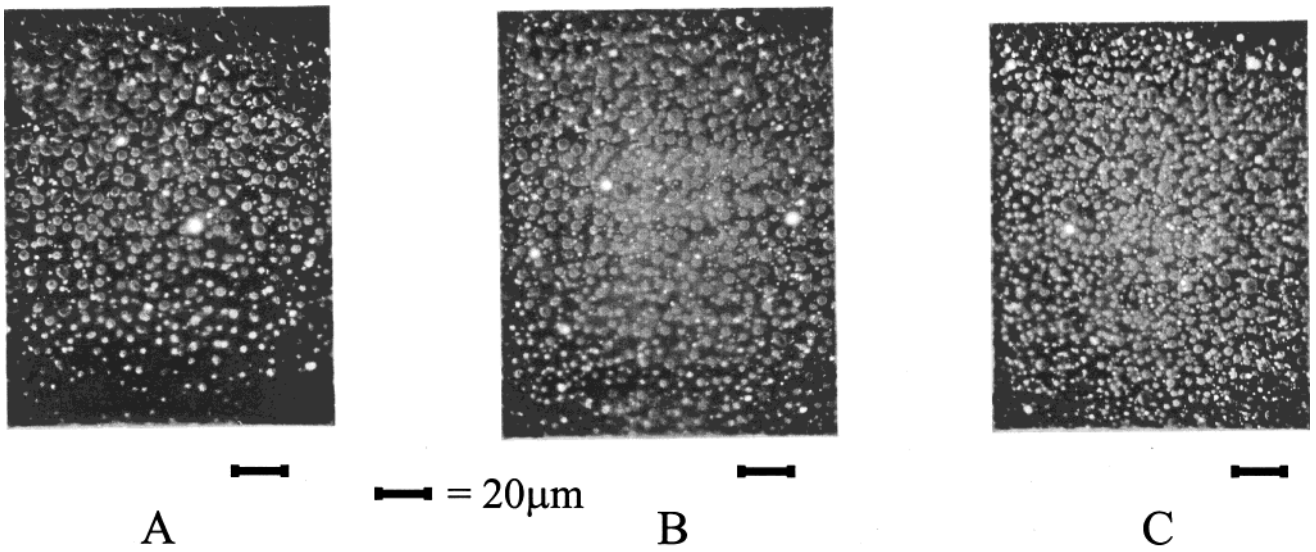

Figure 2. Light microscopy of (A) ES40-5x, (B) ES40-10x, and (C) ES40-35x. Samples were 7 months old at the time of imaging.

for our materials and reflect the different compositional approaches. In the Viers elastomers, optical micrographs of stained sections revealed a spinodal texture with micrometer-scale features indicating phase separation. One feature in common with Viers is the observation of round domains.[19]

To examine compositional dependence, TM-AFM images were obtained (Figure 4) for ES40-5x, -12x, and -35x. These samples are identical to those used for light microscopy described above, but sample age was not uniform. The ES40-5x sample was 7 months old, the 12x sample was 6 months old, and the 35x sample was 5 months old.

The 2D height, phase, and 3D height images in Figure 4 show that all aged PDMS-SD coatings have hemisphere-like surface features. For ES40-2.4x (not shown) only a faint indication of these features is detected by AFM and light microscopy even at aging times as long as 6 months. Thus, the compositional threshold for emergence of surface features is ≥ES40-5x. The island-like features seen in height imaging have diameters up to ∼10 μm, but most are in the 2−5 μm range. The feature height (∼0.6 μm) is exaggerated as the *z* axis is 2 μm while the *x* and *y* axes are 100 μm.

In phase contrast mode, there is relatively little difference in the overall shade of surface features and the matrix background. Considering the pioneering work of Maganov,[36] the overall lack of contrast in phase imaging indicates that there is relatively little difference in modulus of the phase-separated features and the matrix. This suggests that the surface features have moduli similar to the underlying PDMS-SD material. The same data suggest that the composition of the surface features is not radically different from the underlying PDMS-SD material. However, in most phase contrast images, the surface features have alternating circular bands of dark and light shades. These bands may be PDMS-rich and SD-rich domains and are discussed further below.

A model for surface feature development in PDMS-SD materials is shown in Figure 5. The most important element of this model is the diffusion of functional non-network species ("**F**") to the surface. The cartoon shows **F** species with PDMS blocks represented by thin lines and hydroxysiloxane blocks represented by thick lines. The **F** species, whose architecture is unknown but which may include "sol" components or nonreacted low MW components, diffuse to the surface as shown by the arrow. Concentrated at the surface, condensation reactions of $[SiO_x(OH)_{4-2x}]_n$ blocks stabilize the surface microstructures. In addition, it is proposed that the PDMS-rich domains of the surface features sequester nonfunctional species ("**N**") such as cyclics that also diffuse to the surface.

The driving force for the diffusion of non-network species to the surface may be coating shrinkage caused by continued condensation of Si−OH groups in the siliceous domain. That this occurs is supported by solid-state ^{29}Si NMR data on $SiO_{1.45}(OH)_{1.1}$, the siliceous material generated by hydrolysis of ES40. A ^{29}Si NMR

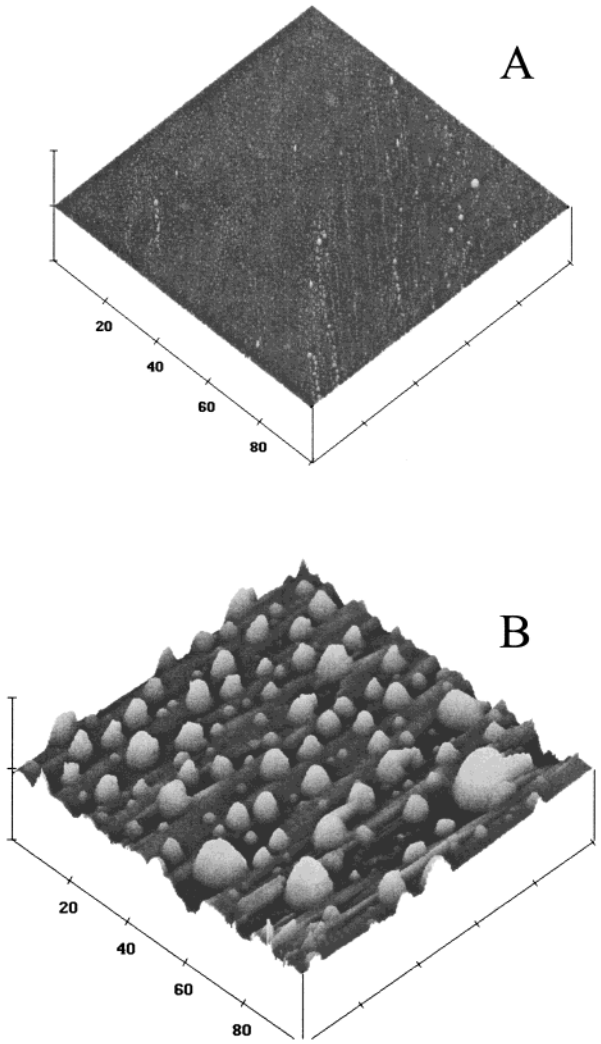

Figure 3. TM-AFM images of ES40-10x after aging (A) 1 month and (B) 6 months (100 μm × 100 μm × 2 μm scan size).

spectrum taken about 1 month after the spectrum shown in Figure 1D (sample stored at ambient temperature) showed an increase in the Q^4 peak at the expense of Q^2 and Q^3 peaks. Thus, the slow evolution of water from condensation reactions in the SD causes shrinkage by virtue of water evolution. Assuming an upper limit of 10 wt % siliceous phase of composition $SiO_{1.5}(OH)$, shrinkage of 1% is calculated for complete dehydration. This shrinkage "extrudes" nonreactive and (surprisingly) reactive non-network species that, concentrated at the surface, slowly form the observed surface features.

A further structural level is proposed on the basis of the circular bands of differing shades observed in phase contrast images of most surface features (Figure 4). The bands vary considerably in width (~1−4 μm), with wider bands appearing on larger features. It is proposed that the alternating dark and light bands arise from alternating layers of PDMS-rich and siliceous-rich domains, respectively. Considering the model in Figure 5, the tip in modulus-sensitive phase imaging mode provides a darker image for band 1, a PDMS-rich domain. For band 2, the tip senses the harder siliceous-rich domain underlying the softer PDMS-rich domain, and the composite modulus is reflected in a lighter image.

Comparison of PDMS-SD and PDMS-FSD Surface Structures. It of interest to compare the AFM images of PDMS-SD materials with those of PDMS hybrid materials prepared with the fluorinated alkoxysilane, (tridecafluoro-1,1,2,2-tetrahydrooctyl)triethoxysilane (FTEOS).[13] Parts A, B, and C of Figure 6 show respectively the 3D height, height, and phase images for FTEOS-6x. FTEOS-6x is a composition that is representative of the range in which "islands" of fluorinated siliceous phase (FSP) are observed. In prior work, it was shown that with increasing FSP content the FSP "islands" merge, ultimately creating a uniform surface monodomain at compositions approximating FTEOS-12x. Thus, compared to PDMS-SD materials, the morphology of the phase separation in PDMS-FSP materials is strongly compositionally dependent. In addition, the topology of PDMS-FSP (Figure 6) is more uniform and reveals more sharply defined domains compared to the surface features of PDMS-SD (Figure 4).

As for PDMS-SD compositions, the formation of domain structures for PDMS-FSP compositions is driven by the formation of a siliceous phase. However, the presence of rodlike fluorinated hydrocarbon groups provides an additional driving force for phase separation in PDMS-FSP materials via the formation of organized structures.[39,40]

Compared to their PDMS-SD analogues, PDMS-FSP compositions show only a modest time-dependent morphological structure. The image of FTEOS-6x shown in Figure 5 is observed on a sample that is 10 months old. Compared with images at an earlier stage (a few months old) reported previously,[13] phase separation has progressed somewhat by the "merging" of smaller islands. The degree of change is slight, however, compared with the features observed on samples a few weeks old. In contrast, surface features on PDMS-SD materials appear only after several weeks.

In summary, PDMS-FSP materials show a phase-separated morphology upon completion of nominal cure (24 h), followed by a small coarsening on a time scale of months. In contrast, PDMS-SD materials initially show no microscale surface features. However, slow evolution of phase-separated surface features occurs over a time scale of months.

Wetting Behavior. As a measure of the extent of surface−water interaction over modest time scales (minutes), we have examined the wetting behavior of silicone containing polymers as a function of immersion time in water.[1,2] To extend this work, the wetting behavior of PDMS-SD materials has been examined.

Figure 7 shows the wetting behavior of pristine samples of ES40-24x. In an attempt to minimize contamination effects discussed below, these samples were made with $HO(Me_2SiO)_nH$ that was extracted with acetone as described in the Experimental Section. At the time of these experiments, the samples were 9 months old. TM-AFM images of ES40-24x show well-developed surface features similar to ES40-14x (Figure 4).

Figure 7 shows six immersion and withdrawal cycles wherein fresh Nanopure water was used for fdc's-a1, -r1, -a2, -r2, -a6, and -r6. Each time the water is changed, the fdc's of the first cycle are reproduced ($\theta_{adv,1}$,/$\theta_{rec,1}$, 114/74). When the water is not changed, the fdc's shift to give lower $\theta_{adv,1}$, 107°, and higher $\theta_{rec,1}$, 81°. The differing protocols show that changing the water, which takes about 10−20 s, "brings back" advancing and receding fdc's that are identical to fdc-a1 and fdc-r1. In separate experiments not shown, fdc-a1 and fdc-r1 data

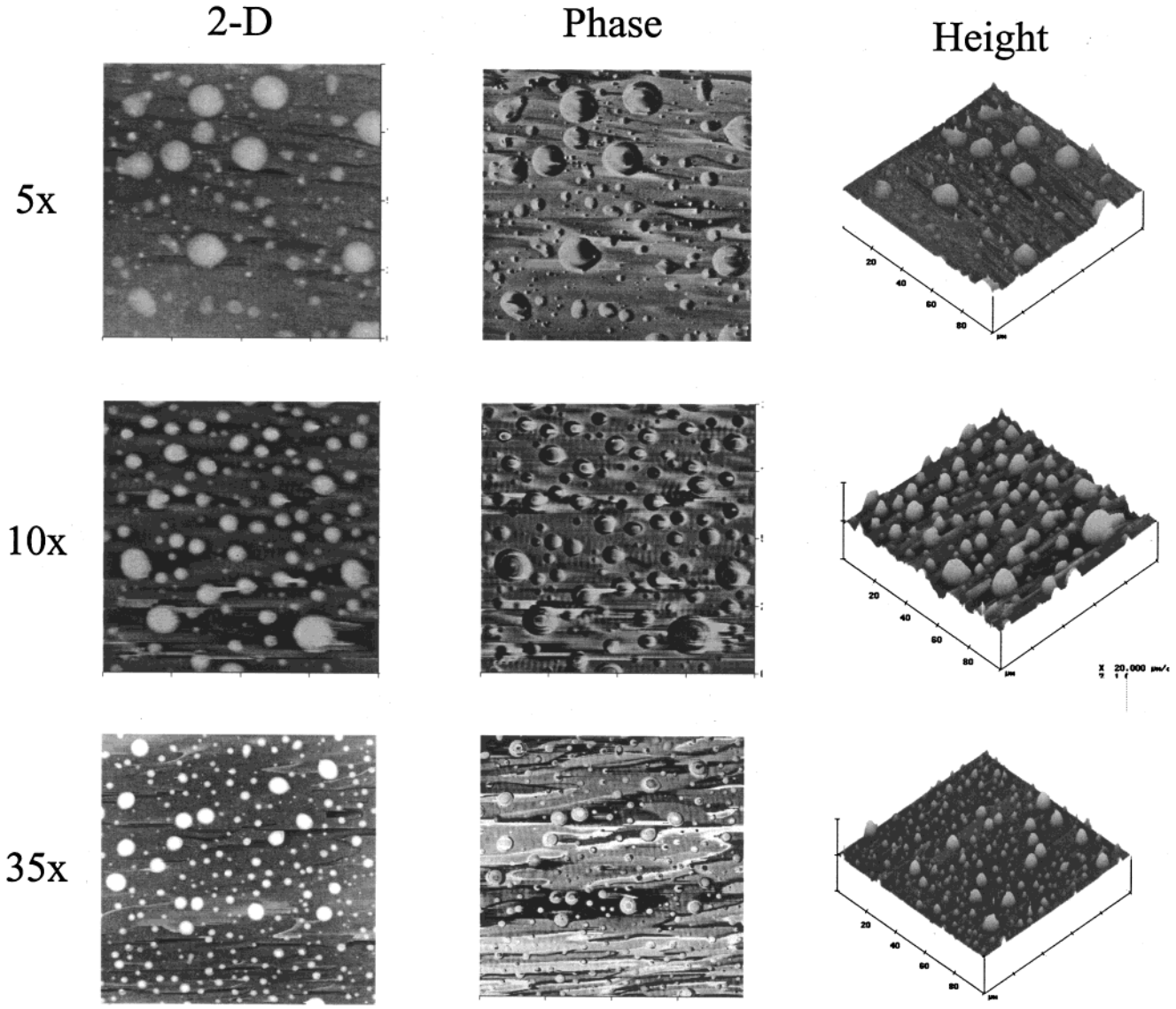

Figure 4. TM-AFM images of PDMS-SD materials. Samples were prepared using unextracted α,ω-dihydroxy functionalized PDMS (100 μm × 100 μm × 2 μm scan size).

are not observed if a pristine sample is interrogated with "used" water. If a clean glass slide is used to interrogate used water, hysteresis characteristic of lowered surface tension is observed.

Finally, the temporal onset of the shift in fdc's is dependent on the surface area of the interrogating liquid reservoir. DCA analysis on a ES40-24x sample utilizing a 50 mL beaker of Nanopure water produced a fdc-1a with $\theta_{adv,1}$ of 115°. When the water was changed before fdc-r1, fdc-r1 showed a break at about halfway through. Receding contact angles depend on whether that portion before the break (71°) or after the break (76°) is used. However, if a larger reservoir of water was used, viz., a 340 mL "crystallizing dish" (d = 96.6 mm), with 6.2 times the surface area of the 50 mL beaker (d = 38.7 mm), three cycles were obtained with identical advancing and receding fdc's ($\theta_{adv,1-3}$,/$\theta_{rec,1-3}$, 115/71).[41] The fourth cycle showed signs of water contamination with lower θ_{adv} and higher θ_{rec}.

Trace amounts of soluble contaminants do not usually produce measurable change in the surface tension of liquids. In the present case some fraction (and we suspect most) of the contaminant is completely insoluble in water and concentrated at the water surface. This contaminant must be silicone oil-like, and though the amounts are small, the effect on surface tension is disproportionately high.

An insidious aspect of this water−surface contamination is that it occurs rather quickly. Depending on the sample, the effect is sometimes seen on fdc-1r, e.g., the ES40-24x sample discussed above. Some samples effectively contaminate the water at a more rapid rate than others. Experiments described below on ES40-12x offer some insight into these observations. Once water contamination occurs, succeeding cycles provide advancing and receding fdc's that are usually superposable as seen for cycles 2, 3, and 4 in Figure 7 and cycles 4 and 5 in Figure 8B. The latter phenomenon led us initially to believe that there was something "irregular" about the first fdc's, but in fact, these fdc's are the only ones providing accurate data on water wettability.

With accurate advancing and receding contact angles, it is seen that the contact angle hysteresis, $\theta_\Delta = \theta_{adv} - \theta_{rec}$, for the PDMS-SD systems is surprisingly high. The ES40-2.4x samples (θ_{adv}/θ_{rec}, 115/71) exhibit a θ_Δ of 44°, while ES40-24x ($\theta_{adv,1}$/$\theta_{rec,1}$, 114/74) have a θ_Δ of 40°. The experimental error in DCA measurements is about ±1°, but we do not have a systematic DCA data set at

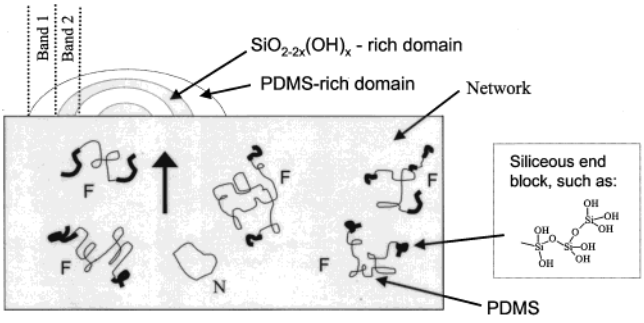

Figure 5. Schematic for generation of PDMS-SD surface features. The closed rectangle represents a cross section of coating, with slow diffusion to the surface of functional nonnetwork siloxane species "**F**" and nonfunctional species such as rings "**N**". One of many possible diffusing **F** species (right-hand corner) is an ABC triblock copolymer comprised of a PDMS block (B) and hydroxysiloxane end blocks (A and C). The side box shows an example of a hydroxysiloxane end block. A representation of the cross section of an island-like surface feature is shown with a layered structured comprised of a siliceous-rich domain and a PDMS-rich domain.

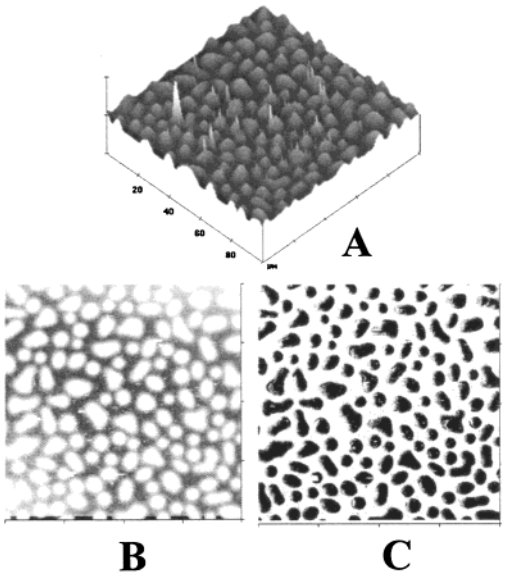

Figure 6. (A) Three-dimensional (3D) height (vertical axis, 2 μm), (B) 2D height, and (C) phase contrast images of FTEOS-6x 10 months after preparation.

well-defined degrees of surface morphology. All that can be said at present is that θ_Δ does not seem to be strongly compositionally dependent.

Surface roughness causes high contact angle hysteresis.[42] PDMS-SD coatings are nominally quite smooth. Table 5 shows the mean-square roughness, R_q, and height range on the *z*-axis for the images in Figure 4. The maximum height range on the *z*-axis is about 1 μm while the maximum R_q is about 90 nm. The lateral dimensions of the surface features depend on sample age but are generally no greater than 5−10 μm. The effect of geometric considerations on θ_Δ is not clear for PDMS-SD materials, but we do not believe that roughness plays a significant role. When geometric considerations play an important role in contact angle hysteresis, quite high θ_{adv} and low θ_{rec} are observed.[42]

It is well-known from the work of Johnson and Dettre that hydrophilic patches on an otherwise hydrophobic surface increases θ_Δ. This pioneering work established experimentally and theoretically that hydrophilic surface heterogeneity on an otherwise hydrophobic surface

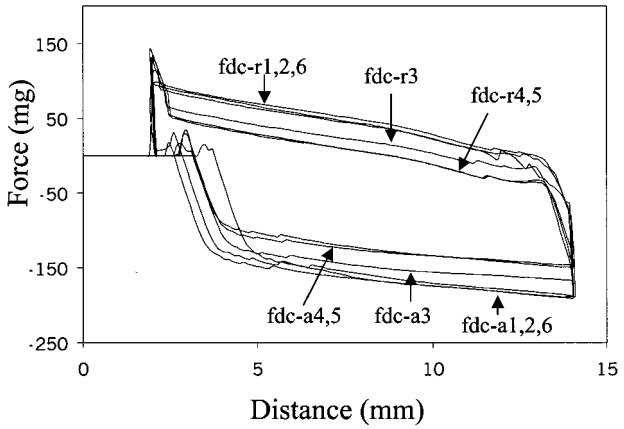

Figure 7. Wetting behavior of ES40-28x with water and beaker changed before fdc-a1, fdc-r1, fdc-a2, fdc-r2, fdc-a6, and fdc-r6.

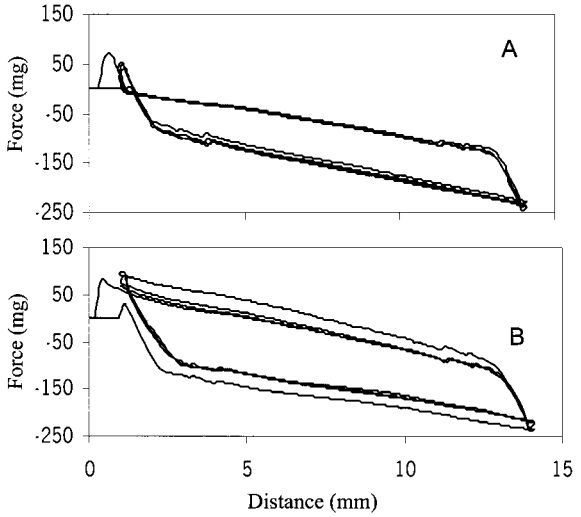

Figure 8. Wetting behavior of ES40-12x with no change of water for all cycles: (A) pristine coating (cured 11 months), $\theta_{adv} = 104°$, $\theta_{rec} = 90°$; (B) cleaned coating, $\theta_{adv,1} = 111°$, $\theta_{rec,1} = 71°$, $\theta_{adv,2-4} = 105°$, $\theta_{rec2-4} = 79°$ (see text).

Table 5. Topographical Roughness Determined by TM-AFM for Images in Figure 3

sample age (months)	ES40 designation	*Z* range (highest to lowest feature, μm)	RMS roughness (R_q), nm
7	5x	0.53	56.8
6	10x	1.1	89.4
5	35x	0.48	48.7

has a minor effect on θ_{adv} but decreases θ_{rec}. Johnson and Dettre explained their observations through a kind of pinning process. That is, up to about 50% coverage, the advancing water front does not "see" the hydrophilic patches. However, once covered by water, the hydrated hydrophilic patches "pin" the receding contact line, water retreats "reluctantly," and θ_{rec} is lowered.

The Johnson and Dettre model for wetting behavior is compatible with our observations of high θ_Δ for PDMS-SD compositions. Once wetted, the near-surface hydrophilic SD or other hydrophilic moieties are driven thermodynamically to the interface. These "hydrophilic patches" pin the receding water line and decrease θ_{rec}.

As noted above, and unlike PDMS-FSP materials, the wetting behavior of PDMS-SD materials was unpredictable. For example, long-aged samples and even some relatively "young" samples did not show the initially high θ_{adv} and low θ_{rec} shown in Figure 6 for ES40-28x.

Despite the use of a 96.6 mm diameter reservoir, DCA measurements on a series of PDMS-SD coatings that were aged for 1 year in air did not display an initially high θ_Δ. These coatings had the characteristic "haziness" caused by the presence of surface features. It was noticed, however, that the portion of the coated slide that was in the water (for a total time of about 20 min) was clear after DCA analysis. Twenty-four hours later, the portion of the slide that had been submerged was again "hazy".

To clarify this behavior, the wetting behavior of an ES40-12x sample (cured 11 months) was investigated. First, the wetting behavior of the "pristine" sample was determined (Figure 8A). Unlike the wetting behavior of the ES40-28x sample discussed above, a repeatable pattern of θ_{adv} and θ_{rec} is observed (θ_{adv}, 104°; θ_{rec}, 90°). After the DCA runs the immersed portion of the coating was clear rather than hazy. The coating was then immersed in additional Nanopure water and gently rubbed with a tissue. The coating, now entirely clear, was subjected to DCA analysis with clean water. Figure 8B reveals quite different wetting behavior compared to the pristine film. The fdc's for the first cycle provide $\theta_{adv} = 111°$ and $\theta_{rec} = 71°$, while subsequent cycles have $\theta_{adv} = 105°$ and $\theta_{rec} = 79°$. The results are explained by water contamination from the surface features on the pristine ES40-12x coating. These features are believed to sequester cyclics and other nonfunctional silicones in the PDMS-rich domains (vida supra). After cleaning, the PDMS-SD coating exhibits wetting behavior similar to ES40-28x described above. It was noted that 24 h later the coating had changed from clear to hazy.

Chemical Stability of Films. Knowledge of both the physical and chemical stability of low surface free energy coatings or films is critical to understanding the interaction with the surrounding medium. *Physical* instability arises from the thermodynamically driven surface reorganization of polar groups to the polymer−water interface.[1] The kinetics of such reorganizations may be fast or slow depending on factors such as proximity of polar functionality to the surface and mobility of the polymer segment bearing the polar functionality. In favorable cases, some idea about the extent of physical reorganization of the polymer surface is gained from evaluation of wetting behavior. For example, we believe that the magnitude of θ_Δ is one measure of the extent of physical surface reorganization that occurs on the time scale of minutes.[39,43]

Chemical instability results from a chemical reaction such as ester hydrolysis. Chemical instability is utilized in ablative coatings containing hydrolyzable polyesters, which prevent the accumulation of fouling by erosion due to hydrolysis.[44,45] Chemical reactivity of polymers is also utilized in drug release.[46] If *intrinsic* relationships to fouling release for low surface free energy surfaces are desired, the surface should not undergo erosion, as intrinsic fouling release characteristics are obscured.

One simple way of evaluating chemical stability is the measurement of coating mass as a function of immersion time in water. Figure 9 shows the total percent weight loss for coatings for PDMS-SD materials prepared from unextracted $HO(Me_2SiO)_nH$ as a function of immersion time. Mass loss from these coatings is compositionally dependent. The highest mass loss occurred for the ES40-35x sample that lost 1.0 wt % after 10 weeks immersion. The second and third highest mass losses over the 10 week study were ES40-28x (0.8 wt %) and ES40-5x (0.6 wt %). Interestingly, a composition of intermediate SD content, ES40-14x, showed the lowest mass loss of 0.24 wt %, or 0.02 wt %/week.

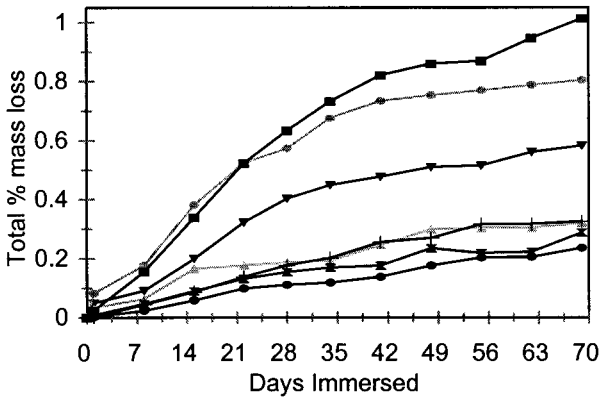

Figure 9. Mass loss data for ES40 samples prepared with unextracted PDMS and 0.18 wt % DBTDA catalyst: ▼ = 5x, ▲ = 10x, + = 12x, ● = 14x, ⋈ = 19x, ○ = 28x, ■ = 35x.

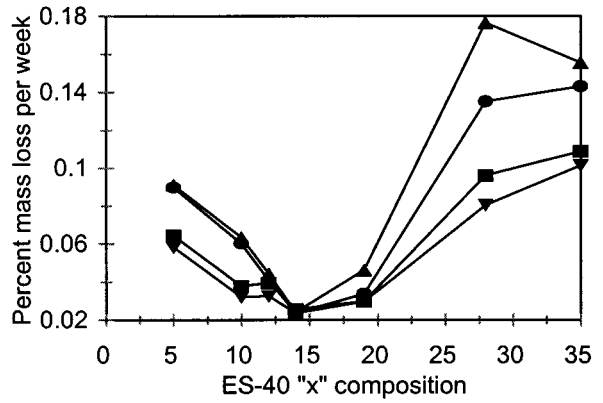

Figure 10. Mass loss trends given in percent mass loss for week for ES40 compositions aged 10 weeks in water at ▲ = 1 week, ● = 5 weeks, ■ = 8 weeks, and ▼ = 10 weeks.

In a related mass loss study for 40 days on coatings prepared with extracted $HO(Me_2SiO)_nH$, ES40-5x samples showed 17% *higher* total mass loss than the unextracted resin. Other compositions had lower total mass loss compared to their unextracted counterparts: ES40-10x, 16% less; ES40-14x, 36% less. The ES40-14x composition prepared from extracted $HO(Me_2SiO)_nH$ exhibited the lowest mass loss (0.09 wt %, 40 days or 0.01_5 wt %/week) of any ethoxysilane-cured $HO(Me_2SiO)_nH$ system that we have examined, including RTV-11.[47]

Figure 10 shows percent mass loss per week as a function of composition. Separate points for mass loss are presented for 1, 5, 8, and 10 week intervals. From these data and from the change in slopes in Figure 9, it is seen that the rate of mass loss for most compositions attenuates with time of immersion. After 10 weeks in water the order of mass loss rate is 35x > 28x > 5x > 10x > 12x > 19x > 14x. The initial rate of mass loss of ES40-14x is low and remains low over the 10 week study. The minimization of mass loss at this composition is puzzling. The Si(−OSi≡)/(OH) ratio in the siliceous domain is not unusual relative to compositions of higher or lower SD content (Figure 1). TM-AFM does not reveal any unique morphology of surface features for this composition.

We have previously evaluated the stability in water of RTV11, a $CaCO_3$ filled, ES40 cured PDMS system

with a stoichiometry approximating "5x". RTV11 has a rate of mass loss of 0.08 wt %/month or 0.02 wt %/week, which was attributed to the slow extraction of low molar mass silicones (LM silicones) including cyclics and linear species. In contrast, a relatively high mass loss is found for ES40-5x composition prepared in this work. The maximum rate of mass loss for ES40-5x occurred during the first few weeks (0.09 wt %/week), while the minimum loss occurred in the last weeks (0.06 wt %/week). The disparate behavior of RTV11 and ES40-5x is not understood, as the time of cure for both materials was comparable.

Relative Stability of PDMS-SD and PDMS-FSP Surface Features. PDMS-SD surface features are fragile relative to those of PDMS-FSP. As noted above, the surface features could be removed by cleaning, and cleaned surfaces showed considerably attenuated water contamination effects compared to the uncleaned sample. Furthermore, it was noted that the cleaning process resulted in a more optically transparent coating. In contrast, cleaning with water as described above did not affect the wetting behavior of PDMS-FSD materials.

Finally, TM-AFM on ES40-10x low set point (0.2 hard tapping) disrupted the surface features, resulting in aligned rows of features in the scanning direction. However, TM-AFM of FTEOS-6x at set point ratios as low as 0.2 did not damage the surface phase-separated structure. TM-AFM data attest to the weak adhesion of the surface features on PDMS-SD materials compared to PDMS-FSP.

Summary

We report PDMS-SD materials with defined compositions. A series of complementary analytical studies that include ^{29}Si NMR spectroscopy, light and AFM microscopy, DCA analysis, and evaluation of mass loss in water provide new insights into surface structure and chemical stability. From ^{29}Si NMR spectroscopy, we learn that the SD generated at ambient temperature with ES40 cure is comprised of varying mole fractions of Q^2, Q^3, and Q^4 silicons. A significant mole fraction of Si−OH is always present in the SD (ca. 0.25).

The initially transparent, hybrid elastomeric PDMS-SD materials become hazy with time because of the slow formation of micrometer-scale, island-like, phase-separated surface features. The PDMS-SD surface features tend to be weakly adherent relative to those of PDMS-FSP. Mechanical rubbing or hard tapping by TM-AFM disturbs or removes the PDMS-SD surface features, whereas similar processes do not damage the PDMS-FSP phase-separated structure. A model for the generation of PDMS-SD features is presented. This model, based on TM-AFM imaging, proposes that the very slow (months) surface structure evolution results from the diffusion of both nonreactive and reactive, non-network PDMS−hydroxysiloxane species to the surface. This is followed by the reactive formation of structures with PDMS-rich and siliceous phase-rich domains.

The wetting behavior of the PDMS-SD materials is complex. For most compositions the surface features contribute to rapid water contamination in DCA experiments. When coatings are cleaned, or in other favorable cases, wetting behavior is characterized by moderately high contact angle hysteresis ($\theta_\Delta \geq 40°$). These relatively high θ_Δ's are explained by a physical surface reorganization in water with the reversible appearance of hydrophilic "patches" of Si−OH containing species (may include PDMS chain ends or siliceous phase fragments) on an otherwise hydrophobic surface.

An evaluation of the stability of PDMS-SD coatings in water demonstrated that the rate of mass loss is minimized for compositions close to ES40-14x. Compositions with higher or lower SD content were more susceptible to mass loss. The unusual maximum in stability for the ES40-14x composition is not understood, as neither SD composition by ^{29}Si SS-NMR nor the surface morphology by TM-AFM reveal unusual features.

Acknowledgment. We thank the Strategic Environmental Research and Development Program (SERDP) and the ONR Scientific Officer Research Program (SORP) for partial support of this research. We are grateful to Dr. T. Ho for GPC data.

References and Notes

(1) Pike, J. K.; Ho, T.; Wynne, K. J. *Chem. Mater.* **1996**, *8*, 856.
(2) Bullock, S.; Johnston, E. E.; Willson, T.; Gatenholm, P.; Wynne, K. J. *J. Colloid Interface Sci.* **1999**, *210*, 18.
(3) Griffith, J. R. U.S. Patent 5,449,553, 1995; U.S. Patent 5,593,732, 1997.
(4) Lindner, E. *Biofouling* **1992**, *6*, 193.
(5) Jalbert, C.; Koberstein, J. T.; Yilgor, I.; Gallagher, P.; Krukonis, V. *Macromolecules* **1993**, *26*, 3069.
(6) Newby, B. Z.; Chaudhury, M. K. *Langmuir* **1998**, *14*, 4865.
(7) Kohl, J. G.; Singer, I. L. *Prog. Org. Coat.* **1999**, *36*, 15.
(8) Kendall, K. *J. Phys. D: Appl. Phys.* **1971**, *4*, 1186.
(9) Compton, R. A. *J. Long-Term Effects Med. Implants* **1997**, *7*, 29.
(10) Milne, A. Anti-fouling marine compositions. U.S. Patent 4,025,693, 1977.
(11) Seeking Clarity on Breast Implants. *Chem. Eng. News* **1998**, *Aug 10*, p 53. National Academy of Sciences, Institute of Medicine, Committee on the Safety of Silicone Breast Implants, 22−24 July 1998, Report, pp 66−71.
(12) Wynne, K. J.; Ho, T.; Johnston, E. E.; Myers, S. A. *Appl. Organomet. Chem.* **1998**, *12*, 763.
(13) Johnston, E.; Bullock, S.; Uilk, J.; Gatenholm, P.; Wynne, K. J. *Macromolecules* **1999**, *32*, 8173.
(14) Wen, J.; Mark, J. E. *J. Appl. Polym. Sci.* **1995**, *58*, 1135.
(15) Hao-Hsin, H.; Orler, B.; Wilkes, G. L. *Macromolecules* **1987**, *20*, 1322.
(16) Huang, T.; Orler, B.; Brennan, A. B.; Wilkes, G. *Chem. Mater.* **1992**, 72, 420.
(17) Gatenholm, P.; Berglin, M.; Johnston, E.; Wynne, K. *Polym. Prepr. (Am. Chem. Soc., Div. Polym. Chem.)* **1998**, *39* (2), 908.
(18) Viers, B. D.; Sukumaran, S.; Beaucage, G.; Mark, J. E. *Polym. Prepr. (Am. Chem. Soc. Div. Polym. Chem.)* **1997**, *38* (2), 333.
(19) Viers, B. D.; Mark, J. E. *Polym. Prepr. (Am. Chem. Soc., Div. Polym. Chem.)* **1998**, *39* (1), 520.
(20) Cihlár, J. *Colloids Surf. A: Physiochem. Eng. Aspects* **1993**, *70*, 253.
(21) Magonov, S. N.; Elings, V.; Papkov, V. S. *Polymer* **1997**, *38*, 297.
(22) Berg, J. C., Ed.; *Wettability*; Marcel Dekker: New York, 1993.
(23) Hogt, A. H.; Gregonis, D. E.; Andrade, J. D.; Kim, S. W.; Dankert, J.; Feijen, J. *J. Colloid Interface Sci.* **1985**, *106*, 289.
(24) Ho, T.; Honeychuck, R. V.; Wynne, K. J. Manuscript in preparation.
(25) The empirical formula is calculated from the Si analysis given in the Gelest catalog, Gelest Incorporated, 612 William Leigh Drive, Tullytown, PA 19007-6308.
(26) Gelest, Inc. catalog, Brinker, C. J., Ed.; p 512.
(27) Diehl, P., Fluck, E., Gunther, H., Kosfeld, R., Seelig, J., Eds. *Solid State NMR II: Inorganic Matter*; Springer-Verlag: New York, 1994.
(28) Lippmaa, E.; Magi, M.; Samoson, A.; Engelhardt, G.; Grimmer, A. R. *J. Am. Chem. Soc.* **1980**, *102*, 4889.
(29) Magi, M.; Lippmaa, E.; Samoson, A.; Engelhardt, G.; Grimmer, A. R. *J. Phys. Chem.* **1984**, *88*, 1518.
(30) Hasegawa, I. *J. Sol.-Gel Sci. Technol.* **1993**, *1*, 57.
(31) Hasegawa, I. *Recent Res. Dev. Pure Appl. Chem.* **1998**, *1*, 573.
(32) Our ES40-1x compositions are optically transparent 1 year after preparation.

(33) Gelest, Inc. catalog, Arkles, B., Ed.; p 498.
(34) *CRC Handbook*, 66th ed.; CRC Press: Boca Raton, FL, 1985; p B-138.
(35) Wawkuschewski, A.; Cantow, H. J.; Maganov, S. N. *Adv. Mater.* **1994**, *6*, 476.
(36) Maganov, S. N.; Elings, V.; Whangbo, M. H. *Surf. Sci. Lett.* **1997**, *375*, 385.
(37) Ge, S.; Takahara, A.; Kajiyama, T. *Langmuir* **1995**, *11*, 1341.
(38) Sauer, B. B.; McLean, R. S.; Thomas, R. R. *Langmuir* **1998**, *14*, 3045.
(39) Katano, Y.; Tomono, H.; Nakajima, T. *Macromolecules* **1994**, *27*, 2342.
(40) Wang, J.; Ober, C. K. *Macromolecules* **1997**, *30*, 7560.
(41) Separate experiments with a related siloxane network have shown that there is no relationship between reservoir volume and the onset of change in advancing and receding fdc's. That is, if a 300 mL "tall beaker" is used, the onset of change in advancing and receding fdc's is similar to that for the 50 mL beaker.
(42) Chen, W.; Fadeev, A. Y.; Hsieh, M. C.; ner, D.; Youngblood, J.; McCarthy, T. J. *Langmuir* **1999**, *15*, 3395.
(43) Holmes-Farley, S. R.; Reamey, R. H.; McCarthy, T. J.; Deutch, J.; Whitesides, G. M. *Langmuir* **1985**, *1*, 725.
(44) Rutkowska, M.; Jastrzbska, M.; Janik, H. *React. Funct. Polym.* **1998**, *38*, 27.
(45) Karlsson, S.; Albertsson, A. C. *J. Macromol. Sci., Pure Appl. Chem.* **1995**, *4*, 599.
(46) Ibim, S. M.; Uhrich, K. E.; Bronson, R.; El-Amin, S. F.; Langer, R. S.; Laurentin, C. T. *Biomaterials* **1998**, *19*, 941.
(47) RTV11 is a trademark of GE Silicones.

MA000023Y